Proceedings of the ASME 2025
Smart Materials, Adaptive Structures, and Intelligent Systems
SMASIS2025
September 8–10, 2025, St. Louis, MO

SMASIS2025-167943

ARTIFICIAL-NEURAL-NETWORK-AIDED MODELING OF 2D PROGRAMMABLE MECHANICAL METAMATERIALS BASED ON EXPERIMENTAL DATASETS

Eric J. Williamson[1,*], Hongcheng Tao[1], Devon P. Scheg[1], Yannik L. Lang[1,2], Francesco Danzi[3], James Gibert[1,*]

[1]Purdue University, West Lafayette, IN
[2]Karlsruhe Institute of Technology, Karlsruhe, Baden-Württemberg, Germany
[3]University of California Merced, Merced, CA

ABSTRACT

Programmable metamaterials have seen increased interest in recent years due to their suitability for a wide range of applications along with the high level of control that they offer over their structural properties. In particular, significant interest has been generated for their application in vibration control as they can be updated and tuned without having to completely rebuild an entire section. However, their complex behavior can make modelling them difficult and time consuming. In recent years, machine learning has emerged as a powerful tool to predict behavior of metamaterials and help reduce the amount of testing time. While prior work demonstrated the efficacy of machine learning on metamaterials with fewer permutations, minimal focus has been placed on its applications for large datasets. This work aims to bridge this gap and demonstrate the possibility of using machine learning algorithms to predict complex metamaterial behavior which is trained on a relatively small dataset. Discussion is also given to a novel approach to collecting experimental data for similar applications.

Keywords: Metamaterials, Machine Learning, Programmable Structures, Material Stiffness

NOMENCLATURE

w	weight for score calculation [dimensionless]
A	Area under the curve [L^2]
F_{max}	Peak force [N]
E	Energy [J]
s	Distance [L]

1. INTRODUCTION

Metamaterials are defined as structures which combine precise design and material properties to yield properties not typically achievable. Commonly, these include optics, magnetism, and mechanical response [1–5]. In recent years, metamaterials have seen increased use in the fields of energy harvesting, vibration isolation, mechanism design, optical cloaking, and countless others owing to their ability to be readily designed for a variety of applications [6–8]. Of particular interest is the use of metamaterials for vibration damping. These systems may be designed to help damp mechanical vibrations or buffer acoustic vibrations [9]. Programmable metamaterials refer to metamaterial structures which may be adapted for a changing environment; rather than being fixed in their function, internal or external stimuli may be used to change some aspect of the configuration to produce a modified response [10–14]. In the context of vibration damping, this can be advantageous owing to the potential altering of the damping profile over time due to viscoelastic material degradation. While programmable metamaterials enable additional capabilities not possible with traditional metamaterials, they can also introduce modeling difficulties because of their complex governing properties. In response to this, some recent work has investigated the use of artificial intelligence (AI) or machine learning (ML) to predict metamaterial behavior without experimentally studying its behavior for all configurations.

Recently, there has been a growing interest in using artificial intelligence (AI) to understand the relationship between metamaterial structures and their output behaviors. A common feature of metamaterial investigations is the need to collect large datasets to sufficiently characterize these highly complex systems. Mohammadnejad et al. explored this challenge by implementing a hybrid data collection approach for training an artificial neural network (ANN), using experimental data to validate a larger finite element (FE)-generated dataset [15]. Their hybrid method was applied to solve an inverse problem; given a stress-strain curve, the ANN was able to predict the architecture of a semi-auxetic metamaterial. Sengodan et al. and Yang et al. both computationally created data sets for their respective metastructures and were able to significantly reduce computational time of a CNN model data points

*Corresponding author: will1904@purdue.edu, jgibert@purdue.edu
Documentation for `asmeconf.cls`: Version 1.41, January 31, 2026.

by using principal component analysis (PCA) [16, 17]. Studies that focus primarily on using simulation-based approaches for data mining are excellent for high-ordered systems, however, due to software availability, computational power, and lack of experimental data for model validation, an alternative data-mining method should be investigated.

In this investigation two novel ideas are introduced, the first of which is a proposed data mining collection method using an automated mechanical device for a programmable stiffness metamaterial. The second is the employment of a constraint-based algorithm for data sampling to achieve a semi-controlled response in large order metamaterial systems. The hypothesis being that using a constrained optimization algorithm can **precondition** the data and outperform stochastic methods in creating the desired metamaterial affect—a buckling failure mode. The significance of this lies in the potential to enable precise, application-specific tuning of metamaterial behavior, thereby advancing their integration into adaptive structures, soft robotics, and energy-absorbing systems. To test this hypothesis, a physics-informed algorithm was implemented and its performance was evaluated against Monte Carlo methods using two complementary approaches. A statistical analysis was conducted to compare the distributions of various material properties in the datasets generated by each method. Further, the predictive accuracy of two ML models was compared on a "forward problem". In this forward problem, the algorithm is given a binary string representing the metamaterial configuration and returns the predicted force / displacement curve. The following sections detail the experimental setup, algorithmic implementation, and comparative results that support this investigation.

2. EXPERIMENTAL DESIGN

This experimental design will cover the manufacturing of the physical device used for the large data set creation, the algorithms used for data set generation, the quantitative process done for post processing data, and lastly the methodology used for the modeling of the CNN.

2.1. Physical Test Bed

The mechanical metamaterial under investigation is a heterogeneous structure consisted of a thin-walled elastomeric matrix forming periodic diamond-shaped unit cells that can be reinforced by selective placement of rigid inclusions, allowing programmability of not only the linear global stiffness but also the comprehensive constitutive relationship under large deformation. While the empty matrix exhibits a monotonic quasi-linear response under compression, connected domains of stiffened unit cells may induce buckling collapses of neighboring zones of empty unit cells, which creates local negative-stiffness regions on the loading curve. The design is formulated using the map from the digital representation of the inclusion patterns, i.e., binary arrays indicating unit cell states as filled ("1") or empty ("0"), to the nonlinear force-displacement response.

The examination of artificial-neural-network-aided design with experimental data is attempted using a finite prototype of the above architecture with 105 unit cells. An image of the test bed for data collection is shown in Figure 1.

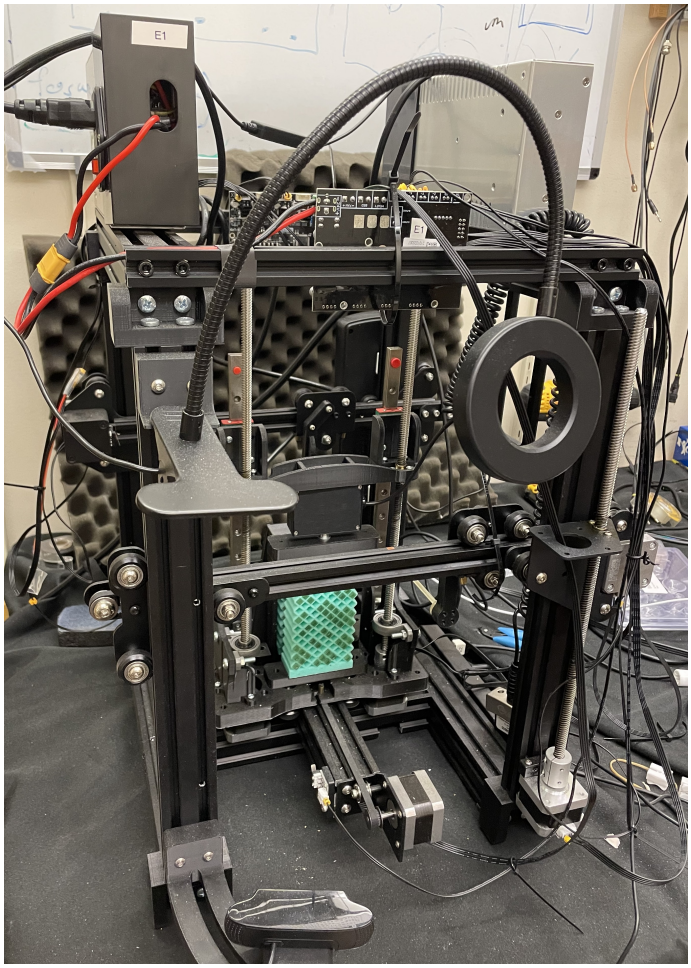

FIGURE 1: IMAGE OF DATA COLLECTION DEVICE

2.2. Dataset Generation

For systems with a large number of degrees of freedom, the workload associated with data collection can rapidly grow. For a system of this size, the number of possible permutations can quickly reach trillions or higher. Because of the sheer number of patterns, physically sampling or modeling a significant fraction of these would be prohibitively costly in time. To combat this, thorough identification of the problem which is being attempted must be completed. For this programmable metamaterial, of particular interest is the buckling behavior which arises due to the interspersed collection of voids and filled cells. By controlling the placement of filled cells, it is hypothesized that the buckling behavior can be precisely controlled to introduce nonlinear stiffness at specific points during the compression of the structure. With this goal in mind, an algorithm was created to form patterns which were made to induce buckling. To begin, a user-selected number of N seeds is randomly placed throughout the grid. This number is subjective and will control the number of buckling paths which may occur in the pattern. From each of these seed cells, the filled pattern will spread to adjacent unfilled cells. This behavior will continue until one of two conditions is met: either the filled cells reach the edge of the structure, or filling a cell will result in it contacting an already filled cell. Once there are

no additional cells to fill based on these criteria, the structure is considered complete. A complete structure visually appears to have cracks running along its face. This pattern allows the unfilled cells to, at times, compress more readily than the filled cells which induces a buckle. In focusing the generation of data to identify patterns, the required amount of data to captured trends is believed to decrease. This can be advantageous and allow a model to be trained on a portion of data which represents only a small fraction of the total number of possibilities.

In this investigation the code would produce a pattern through either a Monte Carlo sample or the aforementioned constrained algorithm and linear actuators would push an inclusions from a 'storage array' into an open cell in the 'testing array'. This same process would happen in reverse if an inclusion needed to be removed based on the automatically supplied distribution code. The testing array would then have a predetermined compression load applied and relaxed. This coupled with a load cell would produce the stress-strain curves for this investigation. It is worth noting that the entire hysteresis curves were not used in data analysis. To reduce computational expense only the loading phase was used and not the unloading half of the experiments. Further, an assumption is made that the material is not plastically deformed under cyclic loading due to a compression load. This assumption is based on the material properties of the silicone rubber used to create the mold; due to its elasticity, these rubbers typically exhibit yield strains at multiple times their lengths, far above what is experienced during the compressive tests studied here [18].

2.3. Data Analysis

The analysis was conducted to examine the relationship between the cell distribution and its resulting force-displacement curve under axial compression. Two different algorithms were used to occupy the cells. One is described in Section 2.2 and the other one is a stochastic placement, both in number and position of the occupied cells. The dataset produced by the algorithm contains 26642 samples, where as the random dataset consists of 5642 samples. The objective was to identify a metric capable of categorizing data from varying cell distribution patterns that yield similar force-displacement responses. This was useful because it gave us insight into features that create a buckling curve, which in turn is valuable information for the forward approach discussed below. The analysis focuses on the force-displacement behavior, buckling phenomena, and spatial distribution patterns observed across the two datasets.

2.4. Dataset Structure

Each subsequent test is composed of two files with one being inclusion patterns and the other being the force and displacement data of the compression test. Each sample is compressed until it reaches 20 N of force; thus, the independent variable is compression force and the dependent variable is compression distance.

The inclusion patterns are represented as a 105 character long binary string for each cell in the lattice structure being 19 rows tall and alternating between five and six cells wide. In said string, each 0 represents an empty cell and each 1 indicates an occupied cell.

To evaluate the similarities between different force-displacement curves, two different metrics were selected based on fundamental aspects of the polymer structure. These metrics were developed to capture distinct characteristics of the response curve and to uncover patterns that could enhance the understanding of buckling behavior within the structure, as well as the factors influencing the overall shape of the curve.

A. Area Under the Curve Energy storage due to strain is commonly studied and parameterized using the strain energy density. For uniaxial strain, the strain energy density can be calculated by evaluating the integral of the stress-strain curve to find its contained area [19]. While the experiment performed herein focuses on force-displacement data, a simple scaling factor would relate it to a stress-strain curve. Thus, for qualitative comparison, strain energy density may be used appropriately. The area under the force-displacement curve was calculated to get a metric that covers the amount of work that was done on the system. Because the compression stops at 20 N for each sample, this metric is driven by the stiffness of each pattern configuration.

B. Number of Force Peaks The secondary value of interest is the number of peaks exhibited in the force displacement curve. When the structure buckles, it will undergo an either temporary or permanent reduction in its force carrying ability which will be reflected in the force-displacement curve. Thus, each local peak in this curve corresponds to a buckling event and knowledge of this buckling can inform further design decisions. Using this metric, structures of different patterns can be categorized into bins of their peak count. Ultimately, the goal is to identify if there are certain structure types which are more or less prone to buckling.

2.5. Forward Problem

For this model, the input was the previously discussed array comprised of ones and zeros. It is noted that the construction of the metamaterial alternates rows of five and six cells. To simplify processing, the pattern was normalized to fit a rectangle with additional imaginary cells being added to fill out the gaps in shorter rows. The final size of the input is 19 rows by 11 columns. The model output was a 1D vector with values representing the normalized displacement exerted during compression. This normalized force produces a value between zero and one; to provide a useful force measurement in Newtons, a basic deep neural network (DNN) was trained in parallel on the same data to predict a scaling value which represents the maximum displacement of the structure. This scaling value is applied to the CNN model to produce a final force vector which can be compared to the experimental test cases. The structure of the neural network is discussed in more detail in Section 3.4

3. RESULTS & DISCUSSION

The analysis of the metamaterial structure datasets reveal key findings regarding the mechanical response and cell distri-

bution patterns of the samples. The results are derived from a combination of histogram analyses [3.1], force-displacement behavior [3.2], and heatmap pattern evaluation 3.3]. Together, these approaches provide an extensive understanding of how cell distribution patterns influence buckling, energy absorption and general deformations in the tested structure.

3.1. Histogram Analysis

A detailed understanding of the geometric and mechanical features across the generated dataset is essential for the interpretation of the results and the following training of the machine learning model. Here, histograms were used to show the distribution of two key metrics across the dataset; area under the curve and number of peaks. The number of bins in each histogram were selected using the Freedman–Diaconis rule to ensure an unbiased resolution of the distribution.

The histogram in Figure 2 captures the amount of buckling within the force-displacement curves across the whole dataset. The plot is very discrete, showing that the maximum amount of peaks found in the dataset never exceeds seven peaks. This confirms that our dataset is not exhibiting excessive noise or other artifacts causing peaks that do not stem from buckling in the structure.

The peak of the distribution shows that most samples exhibit either one or two peaks. This suggests that the majority of structures in the dataset undergo only a single dominant buckling event, while a minority portion of the samples display more complex responses with multiple peaks. The clear discretization by peak count allows for analyses of simple versus more complex mechanical behavior. Having a low amount of samples with more than four peaks reveals either the rarity of intricate configurations, or possibly a selection bias during the generation of the datasets.

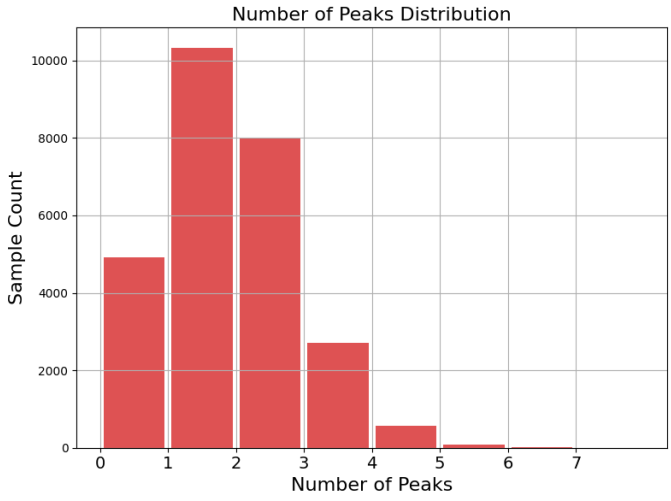

FIGURE 2: DISTRIBUTION OF PEAKS ACROSS THE WHOLE DISPLACEMENT RANGE - ALGORITHM DATASET

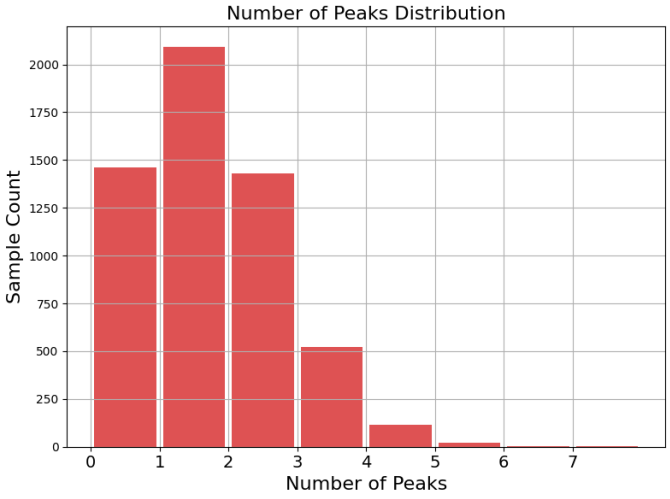

FIGURE 3: DISTRIBUTION OF PEAKS ACROSS THE WHOLE DISPLACEMENT RANGE - RANDOM DATASET

The normalized area under the curve histogram shown in Figure 4 is notably narrow around high normalized values of approximately 0.7. This indicates that despite diversity in peak count and stiffness, the majority of samples are capable of absorbing a substantial amount of mechanical energy, represented by the area under the force-displacement curve ($E = F \cdot s$). This indicates consistent mechanical performance and a robust dataset that does not include outliers.

The lack of samples with a low normalized area suggests that many of the curves are close to the mean, as seen in Figure 6. This subsequently highlights that structures exhibiting significantly more complex force-displacement curves — and consequently larger or smaller areas compared to our test cases — are rare within the dataset. This scarcity may result from inherent physical design constraints or from limitations in the cell placement algorithm, which ensured that no more than 64 cells remained unoccupied; as a result, fully or nearly empty structures were not explored during the experiment.

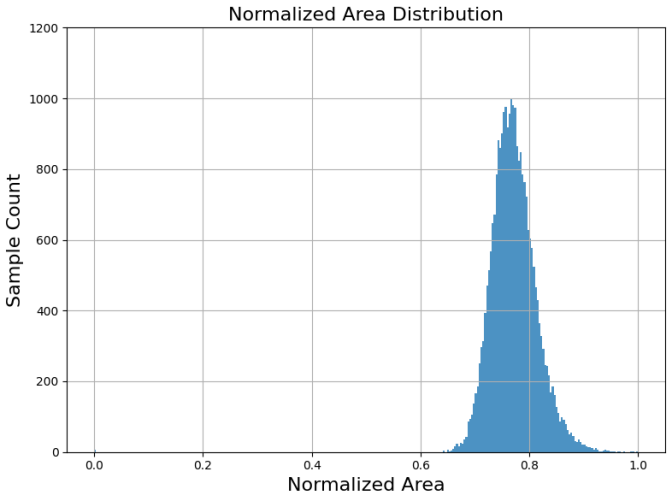

FIGURE 4: DISTRIBUTION AREA UNDER THE CURVE - ALGORITHM DATASET

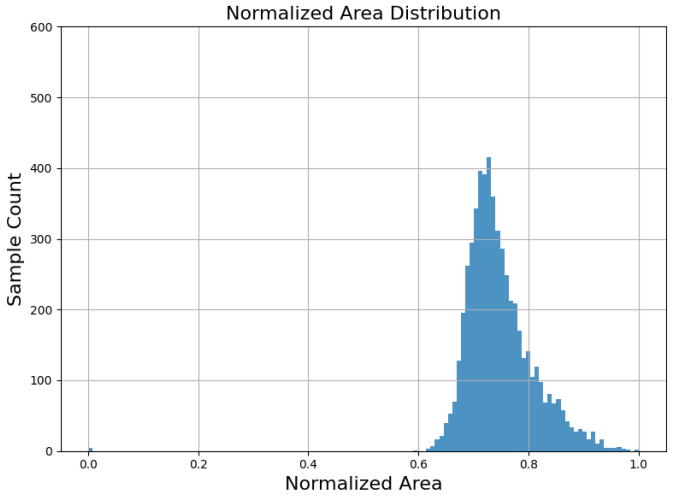

FIGURE 5: DISTRIBUTION AREA UNDER THE CURVE - RANDOM DATASET

3.2. Force-Displacement Behavior

Due to the large amount of experimental data available, it was crucial to find a way to narrow down the batch size to a manageable amount for analysis. Two primary approaches were considered for categorizing the data. The first approach is to group by overall cell count in the structure, which leaves out the information that a specific pattern would exhibit on the mechanical response. The second approach was to inspect each of the 19 rows individually, then creating sub-groups based on the number of occupied cells within each row. Using this method, only the occupancy in the row of interest was considered, while any patterns in the remaining rows were not taken into account.

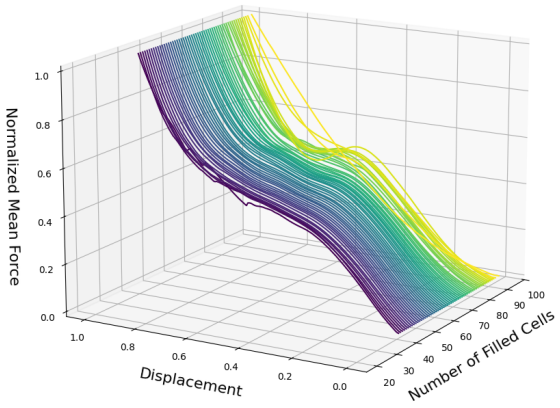

FIGURE 6: DISTRIBUTION OF MEAN FORCE-DISPLACEMENT CURVES ACROSS THE NUMBER OF FILLED CELLS - ALGORITHM DATASET

Figures 6 and 7 present a three-dimensional visualization of mean normalized force-displacement curves (z-axis) as a function of the cell distribution count (number of filled cells - x-axis) and displacement (x-axis) during the compression test. Each colored line represents the mean force response for all samples at a given number of cells occupied, computed across the entire dataset.

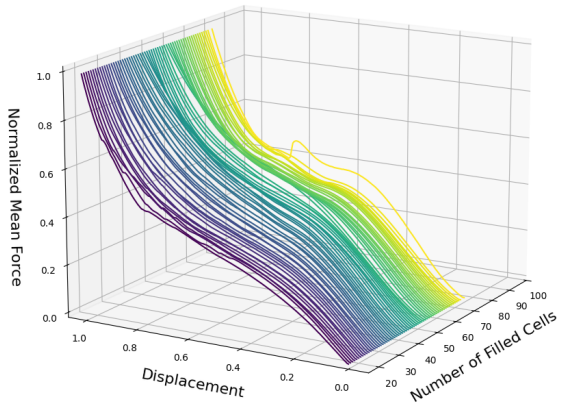

FIGURE 7: DISTRIBUTION OF MEAN FORCE-DISPLACEMENT CURVES ACROSS THE NUMBER OF FILLED CELLS - RANDOM DATASET

	Algorithm Dataset	Random Dataset
Buckling Samples	11071/26642	1996/5642
Percentage	41.6%	35.4%

TABLE 1: BUCKLING IN THE DATASETS

As cell distribution increases, curves generally become steeper near the origin and retain higher force values for longer before declining to a plateau. The drop off after the initial rise also becomes more abrupt in higher cell counts; this may indicate that higher cell counts exhibit more buckling due to their denser cell structures. Moreover, it can be said that the curves display a more complex behavior the more occupied the structure is. This is mostly recognizable in the transitional region near the center of the displacement where the curve goes from a smooth transition to developing more pronounced peaks. However, there are significant outliers. It is believed that these outliers arise from a smaller number of samples with larger numbers of filled cells. Table [1] shows the amount of buckling found in both of the datasets, using a peak height of >0.01 and a minimum distance between two peaks of 10 data points.

3.3. Heatmap and Occupancy Patterns

Heatmaps of the cell distributions provide a visual overview of how cells are distributed within the dataset, and therefore provide a way to gauge the pattern placement algorithm on equal distribution.

The distribution patterns are not random but are the result of the pattern placement algorithm discussed in Section 2.2.

Figure 8a presents a heatmap representing the frequency of

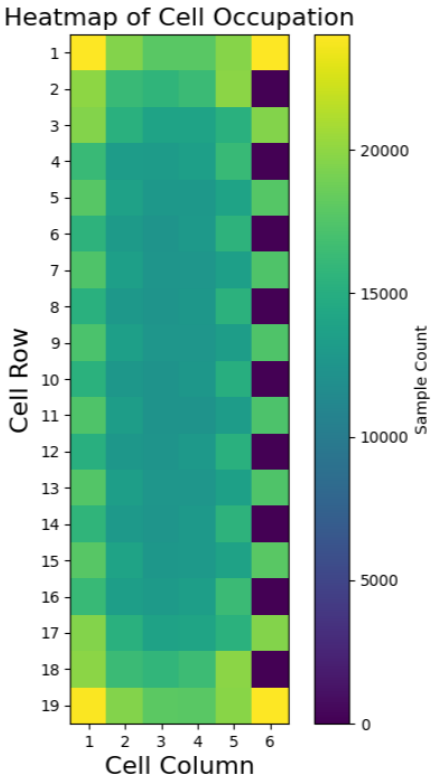

(a) Heatmap - Cell distribution - Algorithm Dataset

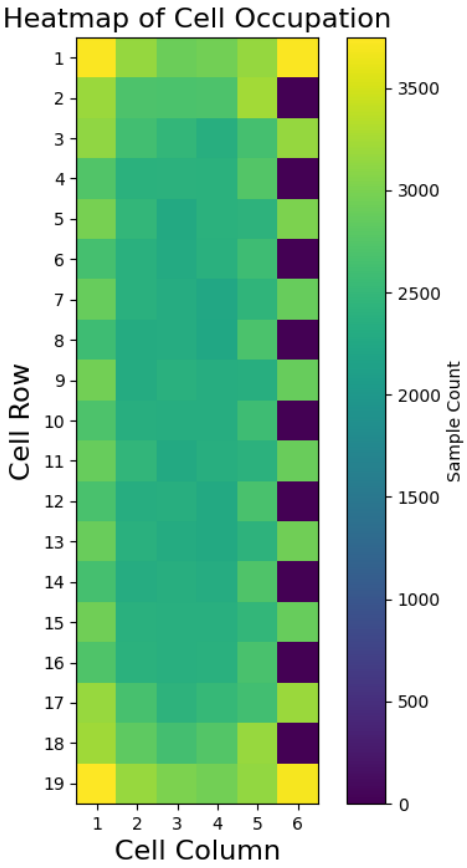

(b) Heatmap - Cell distribution - Random Dataset

FIGURE 8: COMPARISON OF CELL DISTRIBUTIONS ACROSS DATASETS.

distribution for each cell across the entire structure with all 105 cells. The color hereby indicating how often a given cell is filled across all samples.

Note that the actual design involved diamond shape inclusions and cells that alternated between being 5 and 6 cells wide. That is the reason, there is one extra, never occupied cell in each row, compensating for the offset.

The most prominent feature is the extremely high distribution count found at the four corner cells, indicating these sites are filled in almost every configuration. This is likely a result of the pattern placing algorithm. With respect to the algorithm, the central region of the grid (columns 2–5, rows 2–19) is characterized by an even distribution of moderate cell count, slightly increasing in cell count towards the edges. This further undermines the dataset variety in mechanical responses, as there is no real bias to be seen outside of the corners.

3.4. Forward Problem

The forward problem was first tested using a deep neural network. While this yielded accurate force-displacement curves during training, the model performed poorly on a test data set suggesting that the training data had been overfit. Changing the parameters of this model had minimal effect on the outcome, suggesting a limited ability of the model to extrapolate to new data. With this in mind, the model was changed to a CNN. The pipeline of the CNN is shown in Figure 9.
When trained on the algorithm dataset, the CNN performance improved but continued to have significant errors. A representative output of the model is shown in Figure 10.
Generally, the CNN has been found to capture the general shape of the curve well while failing to adequately capture the buckled peaks in the data. Early additional efforts towards refining the CNN parameters have shown some success in improving the performance around these points with a reference output shown in Figure 11. With this improved model, buckling is much better represented though the displacements at which buckling occurs are slightly shifted. These improvements demonstrate the ability of the model to predict complex behavior and lay the ground-

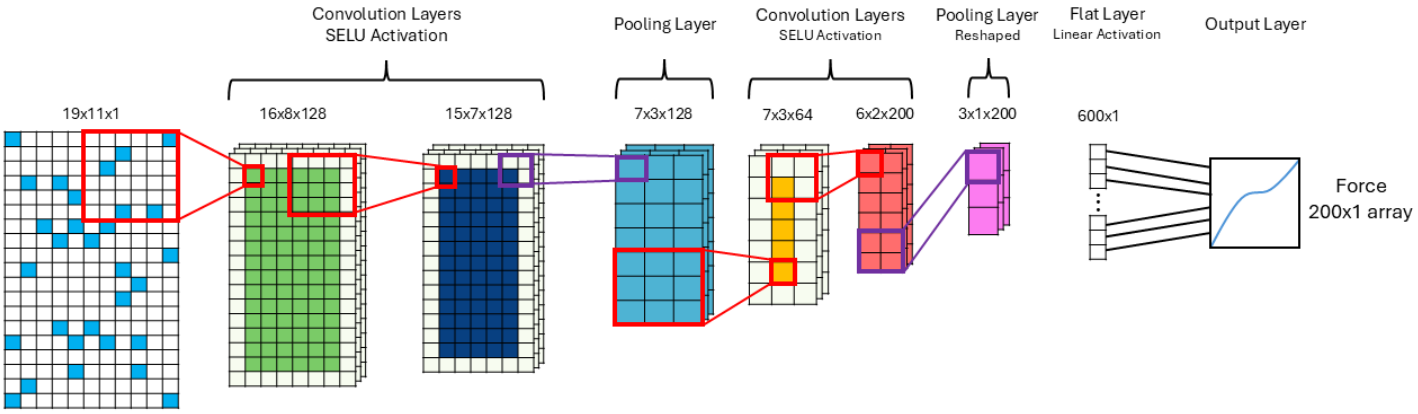

FIGURE 9: INITIAL DESIGN OF THE CNN

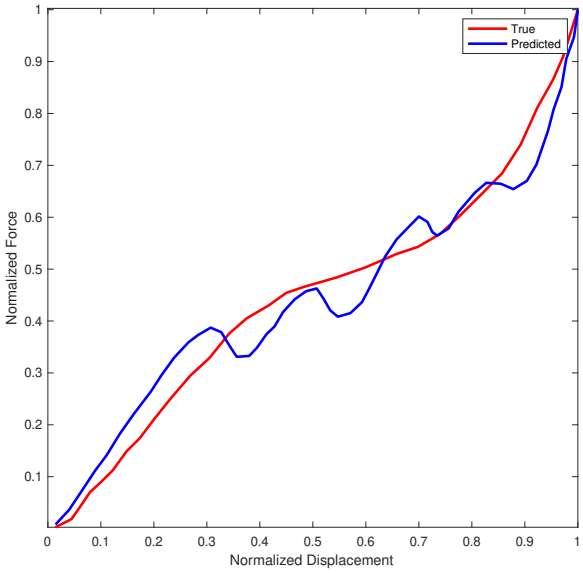

FIGURE 10: EXAMPLE PREDICTION FROM THE 1ST GENERATION CNN

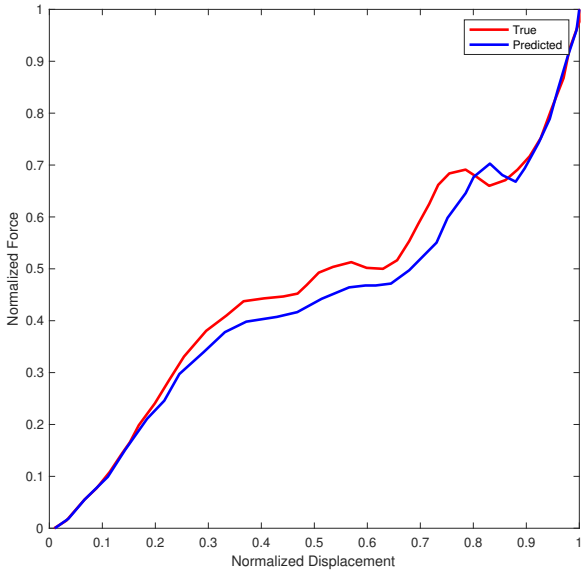

FIGURE 11: EXAMPLE NORMALIZED PREDICTION FROM THE 2ND GENERATION CNN

work for additional efforts. Further work is ongoing to continue refinement and merge the displacement scaling model with this updated CNN.

Work done on similar structures using DNN / CNN models have shown improved results compared to those identified here. Critically, the previously studied structures had fewer cells and were structurally different from the study here. Takagi et al studied a 4x4 metamaterial with cross-shaped inserts and were able to achieve estimated fits with an average R value of 0.995 ± 0.005, distinctly better than the results obtained from the models discussed here [20]. In a similar work, Ma et al studied a similar structure focused on the "reverse problem" of providing a target curve with the model output being the expected pattern. Ma's work showed similar results to the CNN model previously discussed, with the general shape being accurately captured but a decreased ability to differentiate every peak. No existing literature was identified which matched the number of cells or the rectangular shape of the structure which has been studied here.

4. CONCLUSION

The effectiveness of a fully automated data collection mechanism has been demonstrated. This approach enables a "set-and-forget" system for data acquisition, where the primary constraint on data collection speed lies in the performance of the linear actuators. If budgetary constraints are minimal, this limitation can be mitigated by deploying multiple autonomous units to perform parallel data collection. Furthermore, this methodology provides a straightforward framework for algorithmic control, enabling iterative analysis of metamaterials in a manner analogous to finite element analysis (FEA) but with the added benefit of generating physical, empirical data. In addition, by eliminating the need for manual intervention, the dataset will be less prone

to human error. This is particularly important for programmable metamaterials, as experimental repeatability is crucial for optimizing design parameters and ensuring applicability beyond a laboratory setting.

A statistical analysis approach was also employed to identify underlying trends. This enabled a more targeted investigation of the features influencing buckling behavior, which is particularly valuable when designing AI algorithms for controlled buckling in metamaterials. The use of a machine learning algorithm on a metamaterial with this many unique permutations does not appear to have been previously presented in the literature. The ability of the CNN previously discussed to generalize the behavior of these structures is valuable particularly for its ability to generalize large datasets with only a small fraction of the possible permutations of the system in the training set. Prior work with similar metamaterials has utilized smaller grids with fewer total arrangements. This work strengthens the results found through those efforts and demonstrates that similar trends can be extrapolated for larger, non-square metamaterial arrangements. Future work will focus on evaluating material deformation resulting from cyclic loading, with the aim of understanding how repeated use influences the shifting of material properties under consistent insert configurations. Additionally, training a machine learning algorithm to complete the "inverse problem", where a force-displacement curve is given and a structure output is produced, would demonstrate a highly useful ability as it could be used to generate specific force-displacement curves for damping or other applications.

REFERENCES

[1] Wang, Weijin, Sun, Kaixiang, Xue, Ying, Lin, Jie, Fang, Jiukai, Shi, Shengnan, Zhang, Shan and Shi, Yanpeng. "A review of terahertz metamaterial sensors and their applications." *Optics Communications* Vol. 556 (2024): p. 130266.

[2] Pan, Wu, Yan, Yanjun, Ma, Yong and Shen, Dajun. "A terahertz metamaterial based on electromagnetically induced transparency effect and its sensing performance." *Optics Communications* Vol. 431 (2019): pp. 115–119. DOI https://doi.org/10.1016/j.optcom.2018.09.014. URL https://www.sciencedirect.com/science/article/pii/S0030401818307958.

[3] Wang, Zongli, Wang, Xin, Wang, Junlin, Pang, Huizhong, Liu, Suyalatu and Tian, Huqiang. "Independently tunable dual-broadband terahertz absorber based on two-layer graphene metamaterial." *Optik* Vol. 247 (2021): p. 167958.

[4] Dudek, KK, Martínez, JA Iglesias, Hirsinger, L, Kadic, M and Devel, M. "Active magneto-mechanical metamaterial with the wave transmission and Poisson's ratio controlled via the magnetic field." *Journal of Sound and Vibration* Vol. 595 (2025): p. 118784.

[5] Zhang, Yizhi, Hu, Zedong, Neal, Amirr Dion, Mihalko, Claire A, Quigley, Lizabeth, Lu, Ping, Pan, Wei, Paul, Debargha, Tsai, Benson Kunhung, Zhou, Shiyu et al. "Integrating magnetic Co-nanopillars in a NbN-based VAN thin film as a multifunctional hybrid metamaterial." *Materials Horizons* (2025).

[6] Schurig, D., Mock, J. J., Justice, B. J., Cummer, S. A., Pendry, J. B., Starr, A. F. and Smith, D. R. "Metamaterial Electromagnetic Cloak at Microwave Frequencies." *Science* Vol. 314 No. 5801 (2006): pp. 977–980. DOI 10.1126/science.1133628. URL https://www.science.org/doi/10.1126/science.1133628.

[7] Ion, Alexandra, Frohnhofen, Johannes, Wall, Ludwig, Kovacs, Robert, Alistar, Mirela, Lindsay, Jack, Lopes, Pedro, Chen, Hsiang-Ting and Baudisch, Patrick. "Metamaterial Mechanisms." *Proceedings of the 29th Annual Symposium on User Interface Software and Technology*: pp. 529–539. 2016. ACM, New York, NY, USA. DOI 10.1145/2984511.2984540. URL https://dl.acm.org/doi/10.1145/2984511.2984540.

[8] Lu, Ze-Qi, Zhao, Long, Ding, Hu and Chen, Li-Qun. "A dual-functional metamaterial for integrated vibration isolation and energy harvesting." *Journal of Sound and Vibration* Vol. 509 (2021): p. 116251. DOI 10.1016/j.jsv.2021.116251. URL https://linkinghub.elsevier.com/retrieve/pii/S0022460X21003230.

[9] Mei, Chaosheng, Li, Li, Jiang, Yiyuan, Ye, Yuanyuan, Li, Xiaobai, Han, Xiangzhen, Tang, Haishan, Wang, Xuelin and Hu, Yujin. "On band gap and damping of metamaterials involving negative-stiffness elements." *International Journal of Mechanical Sciences* Vol. 239 (2023): p. 107877.

[10] An, Ning, Domel, August G, Zhou, Jinxiong, Rafsanjani, Ahmad and Bertoldi, Katia. "Programmable hierarchical kirigami." *Advanced Functional Materials* Vol. 30 No. 6 (2020): p. 1906711.

[11] Chen, Tian, Pauly, Mark and Reis, Pedro M. "A reprogrammable mechanical metamaterial with stable memory." *Nature* Vol. 589 No. 7842 (2021): pp. 386–390.

[12] Silverberg, Jesse L, Evans, Arthur A, McLeod, Lauren, Hayward, Ryan C, Hull, Thomas, Santangelo, Christian D and Cohen, Itai. "Using origami design principles to fold reprogrammable mechanical metamaterials." *science* Vol. 345 No. 6197 (2014): pp. 647–650.

[13] Liu, Weiqi, Jiang, Hanqing and Chen, Yan. "3D programmable metamaterials based on reconfigurable mechanism modules." *Advanced Functional Materials* Vol. 32 No. 9 (2022): p. 2109865.

[14] Wang, Hairui, Zhao, Danyang, Jin, Yifei, Wang, Minjie, Mukhopadhyay, Tanmoy and You, Zhong. "Modulation of multi-directional auxeticity in hybrid origami metamaterials." *Applied Materials Today* Vol. 20 (2020): p. 100715.

[15] Mohammadnejad, Mohammadreza, Montazeri, Amin, Bahmanpour, Ehsan and Mahnama, Maryam. "Artificial neural networks for inverse design of a semi-auxetic metamaterial." *Thin-Walled Structures* Vol. 200 (2024): p. 111927.

[16] Sengodan, Ganapathi Ammasai. "Prediction of two-phase composite microstructure properties through deep learning of reduced dimensional structure-response data." *Composites Part B: Engineering* Vol. 225 (2021): p. 109282.

[17] Yang, Charles, Kim, Youngsoo, Ryu, Seunghwa and Gu, Grace X. "Prediction of composite microstructure stress-strain curves using convolutional neural networks." *Materials & Design* Vol. 189 (2020): p. 108509.

[18] “Overview of materials for Silicone Rubber.”

[19] Lulay, Kenneth. “Strain Energy Density.” *University of Portland* .

[20] Takagi, Aoi, Ichikawa, Ryo, Miyagawa, Takeru, Song, Jinlan, Yonezu, Akio and Nagatsuka, Hideki. “Machine learning–based estimation method for the mechanical response of composite cellular structures.” *Polymer Testing* Vol. 126 (2023): p. 108161. DOI 10.1016/j.polymertesting.2023.108161.